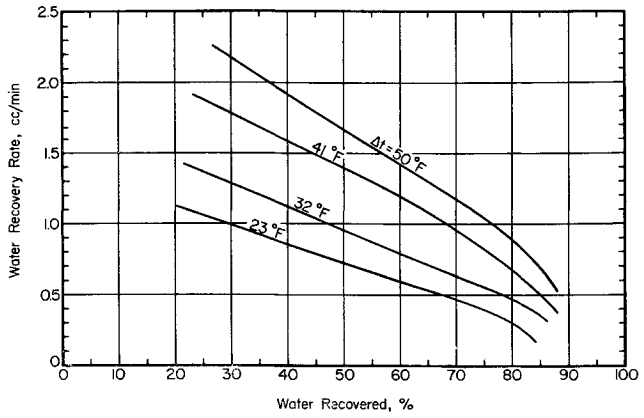

Fig. 3 Relationships between water recovery rate and percent water recovered for various temperature differences.

in., length = 18 in.) to an ice-cooled (32°F) receiver (Fig. 1). Urine was charged into the vaporizer through the feed inlet. The evacuating facilities consisted of a mechanical forepump and a dry ice-acetone vapor trap. The system was evacuated to remove the noncondensable gases. A magnetic stirrer was used in the liquid. The temperature of the vaporizer bath was adjusted to maintain the vaporizer contents at a constant temperature. This arrangement permitted water vapor to escape continuously, without boiling, from the surface of the liquid in the vaporizer to the receiver, where it was liquefied. The temperature difference (Δt) between the vaporizer and condenser dictated the initial rate of water transport to the receiver. However, when these two temperature levels were held constant, the rate of water vapor transport to the condenser gradually decreased while the urine constituents were being concentrated in the vaporizer.

A batch run was conducted at each of four Δt's with 270 cm^3 each of human urine. During the initial evacuating procedure and for the entire duration of the run, no more than 2 cm^3 of water escaped into the dry ice-acetone trap. Once proper vacuum condition was established, the evacuating facility was disconnected from the system. At times, vacuum was applied very briefly to insure the removal of any noncondensables that may have found their way into the system through leaks or through the decomposition of the urine constituents. Considerable difficulty was encountered with runs in which the vaporizer temperature was higher than ambient temperature, because the vapors tended to condense immediately after leaving the liquid surface within the vaporizer and thus decreased the over-all efficiency. This difficulty was eliminated by operating the vaporizer at temperatures somewhat lower than the temperature of the surroundings. The data for the four runs are presented in Fig. 2. Also included in this figure are the recovery relationships of the other three runs. With the exception of run 11, which exhibits an initial unsteady state condition, the recovery vs time relationships are essentially continuous, despite the fact that vacuum was applied in runs 11, 13, and 14 at times indicated by the vertical bars. For run 13, considerable adjustment was required after 75 min of operation to re-establish steady-state conditions. For run 10, no vacuum adjustment was applied over its entire duration of 215 min. With the exclusion of the initial unsteady-state period, the slopes of the curves give the instantaneous rates of water recovery, which are related to percent water recovery in Fig. 3. Because the data are specific to the experimental unit used in this study, no attempt has been made to obtain quantitative projections for the establishment of basic heat-transfer factors and design procedures.

The recovered water was clear but possessed an odor that was still characteristic of urine. A small quantity of carbon black was capable of eliminating the odor. The pH of the untreated water recovered varied with each run from 7.95 to 9.65. After treatment with activated charcoal, the pH approached 9.65 in all cases. Better removal of contaminants probably would follow if an ion-exchange resin were employed in conjunction with the activated charcoal. This mode of treatment was not attempted, but it should produce better potable water.[4]

References

[1] Bambenek, R. A. and Zeff, J. D., "Water recovery in a space cabin," Astronautics **4**, 34–35 (1959).

[2] Golueke, C. G., Oswald, W. J., and McGauhey, P. H., "The biological control of enclosed environments," Sewage and Ind. Wastes **31**, 1125–1142 (1959).

[3] Hendel, F. J., "Recovery of water during space mission," ARS J. **12**, 1847–1859 (1962).

[4] Burm, R. J., "Investigation of the feasibility of urine purification by chemical means," M.S. Thesis, Northwestern Univ., Evanston, Ill. (1962).

Signal Loss vs Antenna Pointing Error

WILLIAM M. BOHANNON*
The Bendix Corporation, Ann Arbor, Mich.

THE design curves presented here relate coverage, beamwidth, antenna pointing accuracy, and signal loss. The geometry from which the analysis proceeds is shown in Fig. 1 for cases where the antenna beamwidth is greater than and equal to the desired coverage. Here, C is the required coverage, measured in degrees. Typical cases would be the angle subtended by the earth from a synchronous satellite (16.4° to 10° elevation ground antennas) or from the lunar surface

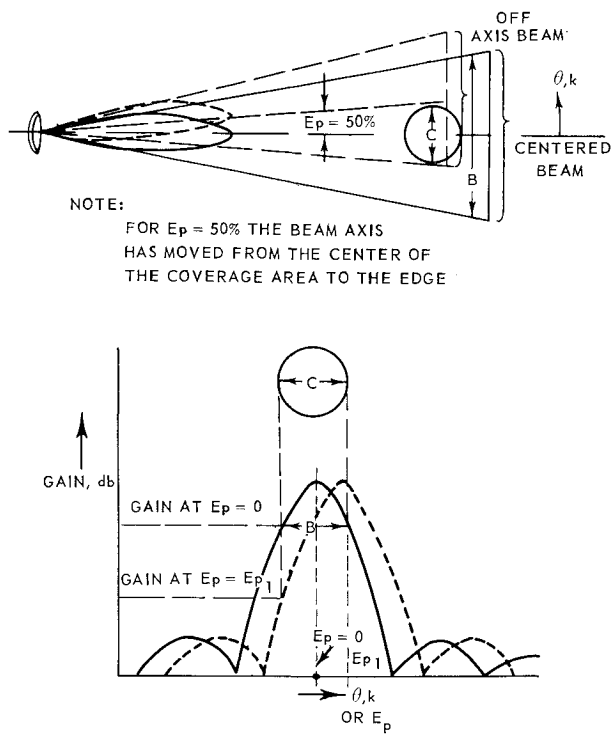

Fig. 1 Geometry for B ≥ C.

Received October 22, 1964; revision received March 10, 1965.
* Systems Engineer, Systems Design Department. Member AIAA.

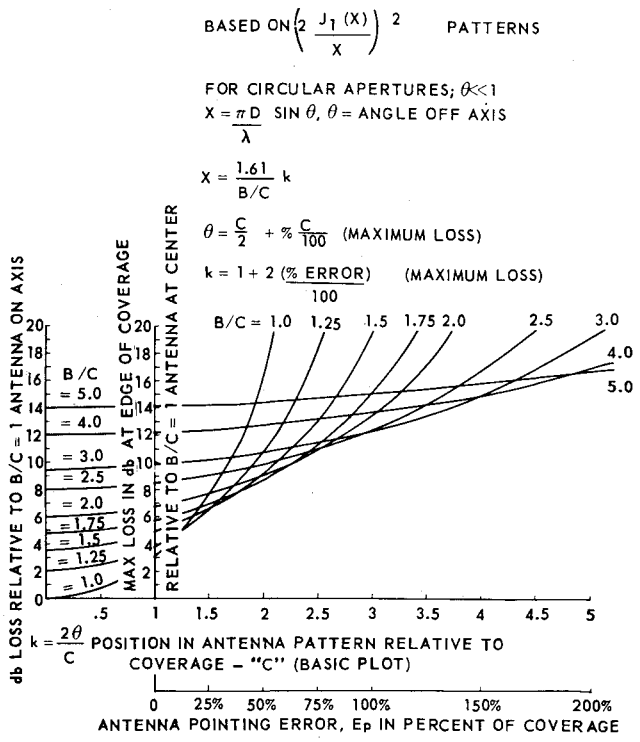

Fig. 2 Signal loss vs angular position in pattern.

(1.8°). The 3-db beamwidth of the antenna is denoted as B; an arbitrary position in the beam as θ; the antenna axis pointing error expressed as a percent of the desired coverage as E_p; and k denotes a position in the pattern relative to $\frac{1}{2}$ the coverage, such that $k = 2\theta/C$.

The first step in plotting signal loss vs beamwidth for various pointing errors was to determine the signal loss incurred as a function of the nondimensional angular position $2\theta/C$ in the beam for various ratios of beamwidth to coverage. The ideal or reference represents the on-axis gain of an antenna with beamwidth equal to coverage with zero pointing error. In this case, shown in the $B/C = 1$ curve in Fig. 2, the edge signal loss at a position one "half coverage" away from center, where $2\theta/C = 1$ is 3 db as expected. For greater values of beamwidth, the loss as a function of position in the beam is less at the edge, but the on-axis value is also less. Figure 2 thus can be used to determine the relative gain at any point in a pattern by careful choice of the value of k.

Figure 2, then, is a series of plots of $[2J_1(X)/X]^2$ with different scale factors determined by the relationships $x = 1.61\ k/(B/C)$. The $[2J_1(X)/X]^2$ factor shown separately in Fig. 3 is the pattern expression for uniformly illuminated cir-

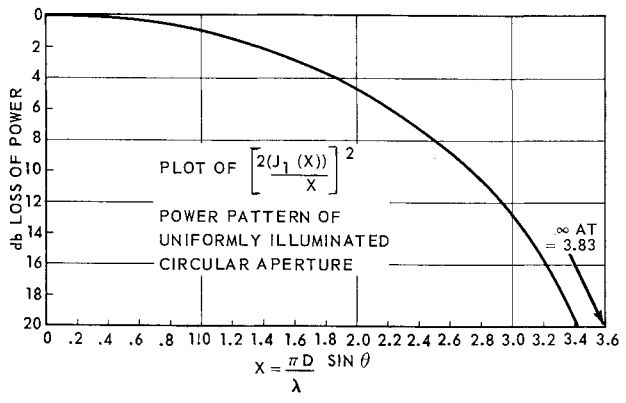

Fig. 3 Plot of [2 J₁ (X)/X]² vs X.

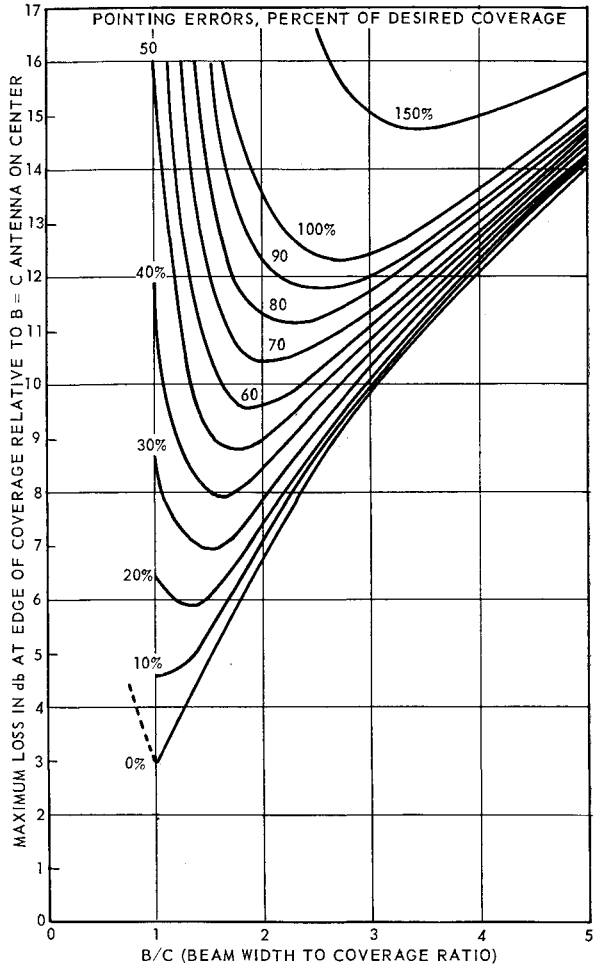

Fig. 4 Maximum loss vs beamwidth-to-coverage ratio for various pointing errors.

cular apertures (with $D/\lambda \gg 1$). The loss values shown here are accurate only to the extent that the approximations $D/\lambda \gg 1$ and $\sin\theta \cong \theta$ are valid.

The next step was to add an abscissa scale to Fig. 2 to generate the loss of gain in decibels at the opposite edge (nominal 3-db point of the coverage area) for antenna pointing errors expressed as percent of the total coverage. The maximum loss error curves start at $2\theta/C = 1$, at which point the error is considered zero. Note that, for maximum loss calculations, $\theta = C/2 + \%\ C/100$ and $k = 1 + 2Ep/100$. For example, the data of Fig. 2 can be used for deep space laser communication system design. For lasers with 10-μrad beamwidth, which just covers the earth at a range of 6.888×10^8 naut miles or nearly 1 a.u., an error of 25% or 2.5 μrad would cause a 7.6-db signal loss at the edge of the earth. The only assumption required for generality of these data is that the antenna (or optics) patterns are defined by the $J_1(X)/X$ patterns in their regions of applicability. (Actually, only small errors will occur if antennas with $\sin X/X$ patterns applicable to rectangular apertures are used instead of the circular apertures used here.)

The final step was the combination of the Fig. 2 data in a form more amenable to antenna pointing requirement analysis. Figure 4 shows the signal loss in decibels at the edge of a coverage area ($2\theta/C = 1$), relative to the on-center signal for a $B = C$ antenna, as a function of B/C for various errors expressed as a percent of desired coverage. The curve is derived by taking vertical profiles at various B/C values for the abscissas of Fig. 2.

The results are quite useful in communication satellite work where antenna pointing is related to attitude control

tolerance. For example, the earth subtends 16.4° to the desired edges of coverage from synchronous altitude. The designer wishes to have as much gain as possible, so he initially sets $B/C = 1$, where $B = 16.4°$ and the maximum full coverage signal gain is 20.1 db. If we refer to Fig. 2, we see that this results in a 3-db loss at the edge for perfect pointing and a 7.6-db loss for 25%, or 4.1° pointing error. With the given pointing error (25%), Fig. 4 shows that the designer would be better off to open the beamwidth to 1.40 times the coverage (or to 23°) and accept a 6.4-db maximum loss (presenting a minimum of 13.7-db signal gain at the edges).

Another application of interest is the case of lunar vehicle communication to the earth, where $C \cong 2°$. For moving vehicles using tracking antennas, the pointing error probably will equal or exceed half the coverage angle, perhaps a 50% or 1° error. Figure 4 shows that the minimum losses occur for $B/C = 1.75$. Thus, a 3.5° beamwidth antenna would be selected for lunar communication if a 50% pointing error existed and all other factors affecting beamwidth were assumed attainable and practical. [At DSIF frequencies, a 3.5° ($B/C = 1.75$) beamwidth antenna would require an 8-ft dish.] The expected minimum gain is 34 db minus 8.8 db (as obtained from the ordinate of Fig. 4 opposite the minimum of the $Ep = 50\%$ curve), or 25.2 db. This is the number that would be used in link calculations and communications system design.

The curves are completely general (within the constraints discussed) and can be used in reverse, that is, they can be used to determine coverage angles where specified signal gains are to be exceeded for given antennas and pointing errors. Thus, given any three of the variables, the optimum value of the fourth can be determined readily.

Meteorological Instrumentation for the Boosted-Arcas Rocket Probe

GLENN CATO*
Electro-Optical Systems, Inc., Pasadena, Calif.

Nomenclature

g = acceleration of gravity
k = Boltzmann constant
m = mean molecular weight
T = absolute temperature
μ = absorption coefficient
ρ = density

Introduction

THE U.S. Naval Missile Center, Point Mugu, Calif., has recently developed a boosted version of the Arcas sounding rocket. The Sidewinder 1A rocket motor is used as the booster. This note describes this rocket probe and suggests measurement techniques and instruments that might be used with it. A complete description of work accomplished on the project is given in Ref. 1. Because the apogee is well above parachute altitudes, instrumentation was sought that would operate during the ascent leg of the trajectory.

The Sidewinder-boosted-Arcas sounding rocket is shown in Fig. 1. It carries the standard Arcas nose cone, which is 20.1 in. long, has an 11.5-in. extension, and provides a payload compartment of about 300 in.^{3} Typical trajectories are shown in Fig. 2.

Presented as Preprint 64-320 at the 1st AIAA Annual Meeting, Washington, D. C., June 29–July 2, 1964; revision received October 13, 1964. Work sponsored by Department of the Navy, Navy Purchasing Office, Los Angeles, Calif., Contract No. N123(61756)32689A(PMR) for the U. S. Naval Missile Center, Point Mugu, Calif.

* Aeronomy Projects Supervisor. Member AIAA.

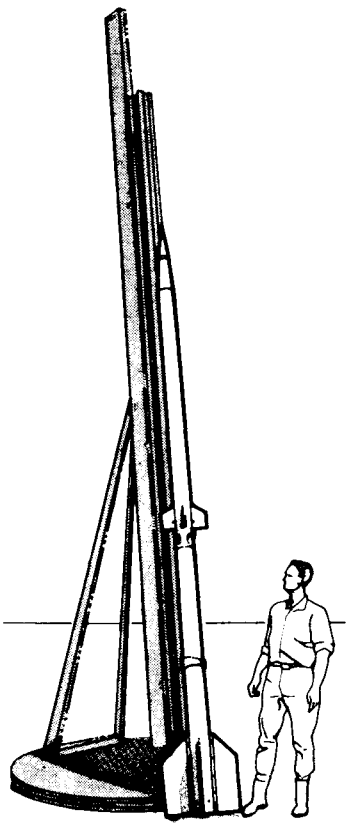

Fig. 1 Sidewinder-boosted-Arcas rocket probe (from photograph supplied by U. S. Naval Missile Center, Point Mugu, Calif.).

Density

Attention was given to the spectrometric technique for the measurement of density. Photometric instrumentation has the advantage of being compact, and the technique has been used successfully with large rockets.

Basically, the instrument measures the intensity and the reduction in intensity of the sunlight due to the absorption of specific solar wavelengths as a function of altitude. Since the amount of absorption depends on the total mass of air above the sensor, it is possible to derive the following relation for density in terms of received energy:

$$\ln\frac{J_2}{J_1} = \mu\int_{h_1}^{h_2} \rho\, dh \qquad (1)$$

where J_1 and J_2 are the measured intensities of sunlight at altitudes h_1 and h_2, respectively.

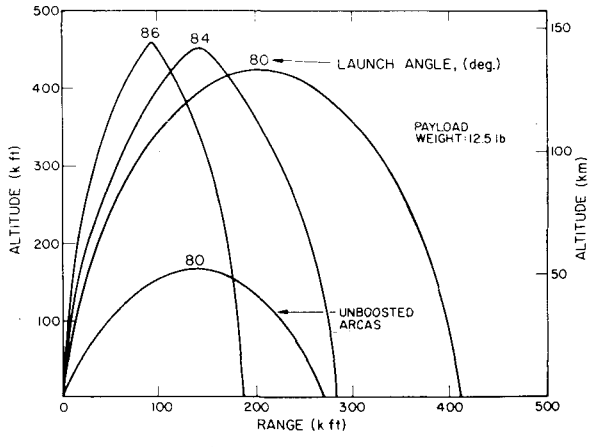

Fig. 2 Sidewinder 1A: Arcas trajectories (data supplied by U. S. Naval Missile Center, Point Mugu, Calif.).